Title
Molecular Imaging of Prostate Cancer Targeting CD46 Using ImmunoPET

Journal
Clinical Cancer Research, 27(5)

ISSN
1078-0432

Authors
Wang, Sinan
Li, Jun
Hua, Jun
et al.

Publication Date
2021-03-01

DOI
10.1158/1078-0432.ccr-20-3310

Peer reviewed

HHS Public Access

Author manuscript

Clin Cancer Res. Author manuscript; available in PMC 2021 September 01.

Published in final edited form as:

Clin Cancer Res. 2021 March 01; 27(5): 1305–1315. doi:10.1158/1078-0432.CCR-20-3310.

Molecular imaging of prostate cancer targeting CD46 using immunoPET

Sinan Wang[1,*], **Jun Li**[2,3,*], **Jun Hua**[2,4,*], **Yang Su**[5], **Denis Beckford-Vera**[1], **Walter Zhao**[1], **Mayuri Jayaraman**[1], **Tony L. Huynh**[1], **Ning Zhao**[1], **Yung-Hua Wang**[1], **Yangjie Huang**[1], **Fujun Qin**[6], **Sui Shen**[7], **Daniel Gioeli**[8,9], **Robert Dreicer**[9,10], **Renuka Sriram**[1], **Emily A. Egusa**[11,12], **Jonathan Chou**[11,12], **Felix Feng**[11,12], **Rahul Aggarwal**[11,13], **Michael J. Evans**[1,11,14], **Youngho Seo**[1,11,12], **Bin Liu**[5,11], **Robert R. Flavell**[1,11,14], **Jiang He**[2,9]

[1]Department of Radiology and Biomedical Imaging, University of California, San Francisco, California, United States.

[2]Department of Radiology and Medical Imaging, University of Virginia, Charlottesville, Virginia, United States.

[3]Department of Nuclear Medicine, Huashan Hospital, Fudan University, Shanghai, China.

[4]Department of Nuclear Medicine, Chongqing University Cancer Hospital, Chongqing, China.

[5]Department of Anesthesia, University of California, San Francisco, California, United States.

[6]Department of Pathology, University of Virginia, Charlottesville, Virginia, United States.

[7]Department of Radiation Oncology, University of Alabama at Birmingham, Birmingham, Alabama, United States.

[8]Department of Microbiology, Immunology, and Cancer Biology, University of Virginia, Charlottesville, Virginia, United States.

[9]University of Virginia Cancer Center, Charlottesville, Virginia, United States.

[10]Departments of Medicine and Urology, University of Virginia, Charlottesville, Virginia, United States.

[11]UCSF Helen Diller Family Comprehensive Cancer Center, San Francisco, California, United States.

[12]Department of Radiation Oncology, University of California, San Francisco, California, United States.

Co-Corresponding Authors: Bin Liu, Department of Anesthesia, University of California, San Francisco, 1001 Potrero Ave, 1305, San Francisco, CA 94110. Phone: +1-415-206-6973. bin.liu@ucsf.edu., Robert R. Flavell, Department of Radiology and Biomedical Imaging, University of California, San Francisco, CA 94143. Phone: +1-415-353-3638. robert.flavell@ucsf.edu., Jiang He, Department of Radiology and Medical Imaging, University of Virginia, Charlottesville, VA 22908. Phone: +1-434-243-1011. jh6qv@hscmail.mcc.virginia.edu.

*:Contributed equally to this manuscript

Disclosure of Potential Conflicts of Interest: BL is a founder and equity holder of Fortis Therapeutics Inc., which licensed intellectual properties from the University of California and is taking the anti-CD46 antibody–drug conjugate to clinical trials. BL, YSeo, and JH hold equity shares in Molecular Imaging and Therapeutics Inc., which were converted to equity shares in Fortis Therapeutics Inc.

[13]Division of Hematology and Oncology, University of California, San Francisco, California, United States.

[14]Department of Pharmaceutical Chemistry, University of California, San Francisco, California, United States.

Abstract

Purpose: We recently identified CD46 as a novel therapeutic target in prostate cancer (PCa). In the present study, we developed a novel CD46-targeted positron emission tomography (PET) radiopharmaceutical, [^{89}Zr]DFO-YS5, and evaluated its performance for immunoPET imaging in murine PCa models.

Experimental design: [^{89}Zr]DFO-YS5 was prepared and its *in vitro* binding affinity for CD46 was measured. ImmunoPET imaging was conducted in male athymic nu/nu mice bearing DU145 (AR-, CD46+, PSMA-) or 22Rv1 (AR+, CD46+, PSMA+) tumors, and NSG mice bearing patient derived adenocarcinoma xenograft LTL-331, and neuroendocrine prostate cancers LTL-331R and LTL-545.

Result: [^{89}Zr]DFO-YS5 binds specifically to the CD46 positive human PCa DU145 and 22Rv1 xenografts. In biodistribution studies, the tumor uptake of [^{89}Zr]DFO-YS5 was 13.3 ± 3.9 % ID/gram and 11.2 ± 2.5 % ID/gram respectively in DU145 and 22Rv1 xenografts 4 days post injection. Notably, [^{89}Zr]DFO-YS5 demonstrated specific uptake in the PSMA and AR-negative DU145 model. [^{89}Zr]DFO-YS5 also showed uptake in the patient-derived LTL-331 and 331R models, with particularly high uptake in the LTL-545 neuroendocrine prostate cancer tumors (18.8 ± 5.3, 12.5 ± 1.8, and 32.0 ± 5.3 % ID/g in LTL-331, LTL-331R, and LTL-545, respectively, at 4 days post injection).

Conclusions: [^{89}Zr]DFO-YS5 is an excellent PET imaging agent across a panel of prostate cancer models, including in both adenocarcinoma and neuroendocrine prostate cancer, both cell line- and patient-derived xenografts, and both PSMA positive and negative tumors. It demonstrates potential for clinical translation as an imaging agent, theranostic platform, and companion biomarker in prostate cancer.

Keywords

CD46; immunoPET; prostate adenocarcinorma; neuroendocrine prostate cancer

Introduction:

Molecular imaging and targeted theranostic agents are playing an increasingly important role in prostate cancer detection and therapy[1]. By pairing a molecular imaging agent labeled with a positron emitting radionuclide with a therapeutic agent such as a beta or alpha radionuclide, molecular imaging may help select patients for appropriate therapy in the context of heterogeneous target expression. In particular, prostate-specific membrane antigen (PSMA) is a well-established biomarker for PCa, making it the target of a number of imaging and therapeutic approaches[2–10]. However, PSMA is not uniformly well expressed in prostate cancer, and in many cases expression is heterogeneous or absent in both localized and metastatic PCa[11–14]. Therefore, there is an unmet clinical need for new theranostic

targets and agents in prostate cancer to facilitate cancer detection and treatment for men with absent or heterogeneous expression of PSMA.

In 2006, we selected phage antibody display libraries on prostate cancer tissues by laser capture microdissection and discovered a panel of human antibodies that target prostate cancer cells residing in their natural tissue microenvironment[15]. Subsequently, we showed by SPECT/CT that one of the selected human antibody fragments efficiently targeted prostate cancer *in vivo*[16]. In 2018 we identified CD46 as the target bound by the antibody, identified the epitope with tumor selectivity and a new panel of CD46 targeting human antibodies, and developed an antibody-drug conjugate (ADC) for prostate cancer therapy[17]. In particular, the lead antibody found in that study, YS5, demonstrated high affinity binding to prostate cancer cell and tissue, with little or no binding to normal tissues except for prostate epithelium and placental trophoblasts. CD46 is known to be a negative regulator of the complement cascade in the innate immune system[18–20]. In contrast with lineage markers such as PSMA, CD46 showed uniformly intense cell surface expression in de-differentiated castration resistant prostate cancer phenotypes including both adenocarcinoma and treatment emergent neuroendocrine prostate cancer. YS5 is a fully human full-length IgG1 and has been developed into an ADC for mCRPC treatment[17]. Currently, the ADC (FOR46) is in a phase 1 clinical trial (NCT03575819). Taken together, these data support the development of a CD46-directed theranostic agent for metastatic prostate cancer.

ImmunoPET is a noninvasive molecular imaging modality which combines the excellent targeting specificity of antibodies or antibody fragments with the superior sensitivity and resolution of PET[4,21,22,]. ^{89}Zr ($T_{1/2}$ = 78.41 h) has been widely used for antibody radiolabeling because its long decay time matches the circulation half-time of full-length antibodies[23–26]. We hypothesize that a CD46-targeted immunoPET radiotracer could enable a whole-body assessment of CD46 expression, evaluate prostate cancer disease burden, and aid patient selection and treatment monitoring for CD46-targeted therapies.

In this study, we report the production and preclinical evaluation of ^{89}Zr-radiolabeled human antibody YS5 ([^{89}Zr]DFO-YS5) as the first immuno-PET probe targeting CD46 positive prostate cancer.

Material and methods:

Compounds and proteins

The fully human CD46-targeted antibody YS5 was produced and purified as previously described[17]. The radiolabeling chelator p-isothiocynate-benzyl-DFO (catalog No. B-705) was purchased from Macrocyclics, Inc (Plano, TX). ^{89}Zr oxalate was purchased from 3D Imaging (Little Rock AR) and the Cyclotron Laboratory at University of Wisconsin, Madison. Recombinant human CD46 Fc chimera protein was purchased from Sino Biological, Inc (Wayne, PA). Native human IgG protein was purchased from ABCAM (Cambridge, MA). Other chemicals were purchased from Sigma-Aldrich, Inc.

Antibody Conjugation and Radiolabeling

Conjugation of p-isothiocynate-benzyl-DFO to YS5: The buffer of 5 mg YS5 was exchanged to 0.1M Na_2CO_3-$NaHCO_3$ buffer pH 9.0 using a 30K MW centrifugal filter. The final volume was adjusted to 1 ml by adding 0.1M Na_2CO_3-$NaHCO_3$ buffer pH 9.0. 1.3 mg p-isothiocynate-benzyl-DFO was dissolved in 208 μl DMSO. 20 μl of the p-isothiocynate-benzyl-DFO solution (5 equivalents to YS5) was added to the 1 ml solution containing 5 mg of YS5. The mixture was incubated at 37° C for 45 mins. The mixture was purified with a PD10 gel filtration column, eluting with 0.25 M sodium acetate solution pH 6.0.

Conjugation of p-isothiocynate-benzyl-DFO to nonspecific IgG was performed, with the procedure similar to the conjugation for YS5.

Radiolabeling: 5 μl (3 mCi) ^{89}Zr oxalate, 5 μl 1M Na_2CO_3, 200 μl 2M NH_4OAc and 200 μg DFO-YS5 were incubated at room temperature for 1 hour. The mixture was subject to iTLC for labeling yield and then purified with a PD10 column eluting with 0.9% normal saline. The final product was also analyzed for purity by iTLC.

Cell Culture

Cell lines were obtained from ATCC. 22Rv1 cells or DU145 cells were maintained in RPMI-1640 medium supplemented with 10% fetal bovine serum (FBS), 100 units of penicillin, and 100 μg/mL streptomycin in a humidified incubator at 37 °C and 5% CO_2. MC38 cells were grown in Dulbecco's Modified Eagle Medium (DMEM) with high glucose, supplemented with 10% FBS, 100 units of penicillin, and 100 μg/mL streptomycin in a humidified incubator at 37 °C and 5% CO_2. Cells were removed from flasks for passage or for transfer to assay plates by incubating them with 0.25% trypsin. Cells were sub-cultured every 3–4 days.

In vitro K_d Measurement

K_d value of [^{89}Zr]DFO-YS5 against CD46 expressing cell line DU145 or 22Rv1 was determined by a saturation binding assay. For the K_d measurement of [^{89}Zr]DFO-YS5 against DU145, DU145 cells were plated in 48-well plates (250 μL/ well) 48 h before testing (triplet) in RPMI1640 medium supplemented with 10% fetal bovine serum. The cell number was about 250,000 per well when the assay was performed. The growth medium was removed and washed with PBS three times. PBS with 1% nonfat milk was added to each well and incubated for 1 hour. The buffer was removed and various concentrations (200 μL/ well, 0.0005–5 nM) of [^{89}Zr]DFO-YS5 in saline were added to cells. The cells were incubated in this buffer for 1 hour at room temperature. Then, the radioactive medium was removed by pipet, cells were washed by PBS twice, and 250 μL of 5N NaOH was added to lyse the cells. The lysate was transferred to 2 ml vials, and the bound radioactivity was counted using a Hidex gamma counter. K_d value was determined by nonlinear regression one site specific binding using GraphPad Prism software (GraphPad Software). For the K_d measurement of [^{89}Zr]DFO-YS5 against 22Rv1, the same procedure was followed except for using 22Rv1 cells instead of DU145.

For the K_d measurement of [^{89}Zr]DFO-YS5 against CD46 recombinant protein, 1 μg/ml CD46 in PBS was placed in an 96 well Nunc MaxiSorp plate (100 μL/ well, Invitrogen) and kept at 4° C for 24 h before testing (triplet). This enables binding of the CD46 protein directly to the plate. The buffer was removed and the wells were washed with PBS for three times. PBS with 1% nonfat milk was added to each well and incubated for 1 hour to minimize subsequent nonspecific protein binding. The buffer was removed and various concentrations (100 μL/ well, 0.0005–5 nM) of [^{89}Zr]DFO-YS5 in saline were added, and incubated for 1 hour at room temperature. Then, the radioactive solution was removed by pipet. The plate was washed with PBS twice, and 250 μL of 5N NaOH was added to denature the protein and remove it and any bound radioactivity from the plate. The solubilized protein bound activity was transferred to small vials, and the bound radioactivity was counted using a Hidex gamma counter. K_d value was determined by nonlinear regression one site specific binding using GraphPad Prism software (GraphPad Software).

CD46 Magnetic Beads Target Binding Fraction Assay

HisPur™ Ni-NTA magnetic beads (catalog No. 88831) was purchased from ThermoFisher Scientific (Waltham, MA). The DynaMag™−2 Magnet (catalog No. 12321D) was purchased from ThermoFisher Scientific (Waltham, MA). To 40 ml PBS 20 μl tween20 was added to make the PBST solution. Vials were divided as testing group A, blocking group B and control group C (triplicate in each group). 20 ul HisPur™ Ni-NTA magnetic beads and 380 ul PBST was added to the vials in group A, B and C. Samples were vortexed, beads were trapped by the DynaMag™−2 Magnet and the supernatant was removed. 360 μl PBST and 40 μl 25 μg/ml CD46 was added to group A, B and C, the supernatant was removed and the beads were washed by PBST once. 2 ng [^{89}Zr]DFO-YS5 in 1% milk PBS was added to Group A and B, 2 ng [^{89}Zr]DFO-IgG was added to group C. 10 μg YS5 antibody was added to the blocking group B. Samples were diluted to 400 μl/vial using 1% milk PBS, incubated for 30 minutes, washed with 1% milk PBS twice. The activity of beads, 2 ng [^{89}Zr]DFO-YS5 and 2 ng [^{89}Zr]DFO-IgG was read using Hidex gamma counter. Binding percentage was calculated by beads activity/2 ng [^{89}Zr]DFO-YS5 activity for group A and B or beads activity/2 ng [^{89}Zr]DFO-IgG activity of group C.

Xenograft Models

All animal studies were conducted according to Institutional Animal Care & Use Program (IACUC) approved protocols at University of California, San Francisco and University of Virginia. Male 5–6 week old athymic mice (nu/nu, homozygous; purchased from Jackson Laboratories or Charles River) were housed under aseptic conditions, and received subcutaneous tumor cell inoculation. In brief, 3–5 million cells in a 200 μL 1:1 mixture of complete medium and matrigel (Fisher Scientific, IL) was injected in the thigh or shoulder of the animals. All mice were subjected to undergo PET imaging as well as biodistribution analysis when the tumor reached a size of 300–500 mm^3.

The LTL-331, LTL-331R, and LTL-545 patient-derived xenograft (PDX) were obtained from the Living Tumor Laboratory (Vancouver, CA)[27]. In brief, PDX tissue (~5mm × 5mm) was passaged in intact NOD/SCID/gamma mice subcutaneously. Mice were subjected to

PET imaging as well as biodistribution analysis when the tumor reached a size of 300–500 mm^3.

In Vivo [^{89}Zr]DFO-YS5 and [^{68}Ga]Ga-PSMA-11 PET Imaging Studies

Approximately 3–5 weeks after tumor implantation, animals with tumors reaching 300–500 mm^3 were anesthetized by isoflurane inhalation. For [^{68}Ga]Ga-PSMA-11 PET/CT imaging, methods were identical to those previously reported[28]. For [^{89}Zr]DFO-YS5 PET imaging, 3.70–5.55 MBq (100–150 μCi, 10 μg/mouse) of [^{89}Zr]DFO-YS5 in saline was administered through tail vein. The animals were imaged at various time points with a 20-min acquisition time by using microPET/CT (Inveon, Siemens Medical Solutions, Malvern, PA) or Albira trimodal PET/SPECT/CT scanner (Bruker Corporation, Billerica, MA). PET imaging data were acquired in list mode and reconstructed using an iterative 2D OSEM reconstruction algorithm (for Inveon data) or Albira Software Suite (for Albira data) provided by the manufacturer. The resulting image data were then normalized to the administered activity to parameterize images in terms of %ID/ml. Imaging data were viewed and processed using an open source Amide software. CT images were acquired following PET, and the CT data were used for attenuation correction for PET reconstruction, and anatomical reference.

For the serial PET imaging study of DU145 tumor detection, PET images were acquired at 24 h, 48 h, 72 h, 96 h, 120 h, 144 h and 168 h in tumor-bearing mice post-injection of [^{89}Zr]DFO-YS5 (3.7–7.4 MBq [100–200 μCi]).

To validate the specificity of tumor targeting, PET imaging were also performed at 24 h, 48 h, 72 h and 96 h post-injection of [^{89}Zr]DFO-YS5(5.92–7.03 MBq [160–190 μCi]) with groups of mice bearing both DU145 (target positive) and MC38 (target negative) tumors. As another blocking control, a group of mice with DU145 received 300 μg of unlabeled YS5 at 48 hours before the injection of [^{89}Zr]DFO-YS5 5.92–7.03 MBq [160–190 μCi]), followed by PET imaging at 48 h later. As a comparison of the tumor targeting, a control monoclonal antibody IgG (non-binding control) was also radiolabeled with ^{89}Zr ([^{89}Zr]DFO-IgG) in the same process and the PET imaging of DU145 tumor bearing mice was recorded at 48 hours followed by terminal biodistribution study.

Biodistribution Studies

The tumor bearing mice were sacrificed at various time points post injection of [^{89}Zr]DFO-YS5. Blood was collected by cardiac puncture. Major organs (liver, heart, kidney, lung, spleen, stomach, small intestine, large intestine, pancreas, muscle, subcutaneous tumor and bone) were harvested, weighed, and counted in an automated gamma counter (Hidex). The percent injected dose per gram of tissue (% ID/g) was calculated by comparing with standards of known radioactivity.

Autoradiography

4 days post-injection of [^{89}Zr]DFO-YS5, mice were sacrificed and tissues were immediately collected and flash frozen in OCT on dry ice. Tissues were sectioned on a microtome at a thickness of 20 μm and immediately mounted on glass slides. The slides were then exposed on a GE phosphor storage screen for 1 hour, and the screen was developed on an Amersham

Typhoon 9400 phosphor imager. The autoradiography images were processed using ImageJ software.

Flow cytometry

Cell surface CD46 expression was analyzed by flow cytometry using methods described previously[17]. Briefly, the YS5 IgG1 was conjugated to Alexa Fluor 647® using an Alexa Fluor 647® Monoclonal Antibody Labeling Kit (Thermo Fisher Scientific) according to manufacturer's instructions. Alexa Fluor 647®-labeled YS5 IgG1 was incubated with monodispersed cells isolated from PDXs (LTL-331, LTL-331R, and LTL-545) at room temperature for 1h, and washed three times with PBS to remove unbound antibody. Binding was analyzed by flow cytometry (BD Accuri C6, BD Biosciences) with median fluorescence intensity (MFI) recorded for each sample.

Statistical Analysis

Data were analyzed using the unpaired, 2-tailed Student t test and one-way analysis of variance (ANOVA). Differences at the 95% confidence level ($P < 0.05$) were considered to be statistically significant.

Results:

Synthesis and *in vitro* analysis of [^{89}Zr]DFO-YS5

The radiolabeling of ^{89}Zr oxalate to DFO-YS5 was accomplished in a typical, two step procedure by first conjugating with desferoximine (DFO), and then subsequent chelation of the isotope (Figure 1A). Using 5 equivalents of p-SCN-Bn-DFO, an average of 1.33 chelators were added to the antibody, as determined by MALDI-MS (Supplementary figure S1). The intermediate DFO-YS5 could be stored at −20°C for 12 months without detectable loss of binding activity after radiolabeling with ^{89}Zr. [^{89}Zr]DFO-YS5 was isolated in 74 ± 11% (n = 6) yield based on starting ^{89}Zr oxalate with molar activities ranging from 274.2 – 351.1 MBq/mg (39.7 – 50.8 GBq/μmol, 7.42 – 9.49 mCi/mg, 1.07 – 1.37 Ci/μmol). Radiopharmaceutical purity was greater than 95% in all cases (Figure 1B). Size exclusion chromatography demonstrated no evidence of aggregation (Supplementary figure S2).

The binding affinity of [^{89}Zr]DFO-YS5 was measured in a saturation binding assay by incubating CD46 expressing cell lines or recombinant CD46 with increasing concentration of [^{89}Zr]DFO-YS5. The dissociation constant value K_d was 6.7 ± 0.3 nM for DU145 cell line, 7.2 ± 0.9 nM for 22Rv1 cell line and 6.0 ± 0.6 nM for a recombinant CD46 protein (Figures 1C, 1D and 1E). A competition radioligand binding assay was developed using [^{89}Zr]DFO-YS5, in the presence of varying concentrations of competing YS5 or DFO-YS5. In this assay, the IC_{50} for YS5 was 23.1 ± 1.8 nM, and for DFO-YS5 was 37.8 ± 2.5 nM (Figure 1F). We adopted a recently described magnetic bead based radioligand binding assay to determine the target binding fraction of the labeled [^{89}Zr]DFO-YS5 (Figure 1G). In this assay, the binding of [^{89}Zr]DFO-YS5 was 79.5 ± 2.0 %, while marked reductions were seen in the presence of 10 fold excess of cold YS5 to 18.4 ± 1.8%. Nonspecific IgG demonstrated minimal binding of 5.2 ± 3.6%. Taken together, these data demonstrate that [^{89}Zr]DFO-YS5

can be synthesized in an efficient, reproducible manner, with minimal loss of binding affinity.

Longitudinal PET imaging and biodistribution analysis of [^{89}Zr]DFO-YS5 in DU145 tumor model

ImmunoPET images of [^{89}Zr]DFO-YS5 recorded in DU145 tumor–bearing mice between 24 to 168 h are presented in Figure 2, supplemental Figure S3 and on supplemental table S1. The *in vivo* tumor targeting of [^{89}Zr]DFO-YS5 was also quantified by conducting biodistribution studies in DU145 tumor-bearing mice at 24 h, 48 h, 72 h, 96 h, and 168 h after IV administration. The data revealed that high DU145 tumor uptake was observed at 24 h (11.4±2.6 %ID/gram), with a steady increase through 48 h (14.1±1.8 %ID/gram) and 72 h (14.8±4.6 %ID/gram) and reaching 18.2±10.9 %ID/gram at 168 h (Figure 2B). This gradually increasing accumulation of [^{89}Zr]DFO-YS5 in tumor is along with the extraction of the activity from the blood (24 h, 10.9±1.4 %ID/gram; 48 h, 5.7±0.9 %ID/gram; 72 h, 3.0±0.4 %ID/gram; 96 h, 2.0±0.3 %ID/gram and 168 h, 3.0±0.3 %ID/gram). These increasing tumor uptake correspond with high tumor/muscle ratios of 15.6±7.5, 26.3±4.7, 19.4±2.2, 59.0±16.5, 53.6 ±42.3 for the times at 24 h, 48 h, 72 h, 96 h, and 168 h, respectively (Figure 2C).

Comparison of [^{89}Zr]DFO-YS5 and [^{68}Ga]PSMA-11 PET/CT in the CD46 and PSMA positive 22Rv1 xenograft model

To further evaluate the imaging ability of [^{89}Zr]DFO-YS5, and compare it to the PSMA based prostate cancer imaging agent [^{68}Ga]PSMA-11, [^{89}Zr]DFO-YS5 or [^{68}Ga]PSMA-11 were administered to athymic mice xenografted with 22Rv1 cells subcutaneously. Mice administered with [^{89}Zr]DFO-YS5 were imaged 4 days post IV injection and then sacrificed for a biodistribution study. As shown in Figure 3A, the probe specifically localized at the tumor site and had a low accumulation at other organs. The biodistribution study showed that the tumor uptake was 14.5 ± 3.2 % ID/gram at 4 days post injection, whereas the uptake at other organs was all below 5% (Figure 3B, Supplemental table S2). Mice administered with [^{68}Ga]PSMA-11 were imaged 1 hour post IV injection and then sacrificed for a biodistribution study. As shown in Figure 3C, and as expected based on our own prior study[28], the [^{68}Ga]PSMA-11 demonstrated high tumor, spleen, and especially kidney uptake. The biodistribution study showed 3.74 ± 0.76 % ID/gram uptake at tumor and over 120% ID/gram uptake at kidney because of its high expression level of PSMA (Figure 3D, Supplemental table S2). These results demonstrate that [^{89}Zr]DFO-YS5 can specifically image CD46 positive prostate cancer with favorable imaging characteristics compared to [^{68}Ga]PSMA-11 in the 22Rv1 model.

Specificity of CD46 tumor targeting *in vivo*: PET imaging and biodistribution in CD46+ and CD46- negative tumors, together with blocking and control antibody studies

In order to verify the specificity of CD46 targeting of [^{89}Zr]DFO-YS5, a series of control experiments were performed, including imaging in CD46 negative tumors, a blocking study, and comparison with a control, non-binding antibody. Biodistribution studies using a non-binding, control antibody IgG group and a blocking group were compared against [^{89}Zr]DFO-YS5 alone in the DU145 model (Figure 4: A and B, Supplemental table S3). As

expected, high targeting of [^{89}Zr]DFO-YS5 was observed with tumor uptake at 14.1±1.8 %ID/gram at 48 h post-injection. In contrast, much lower tumor uptake using non-binding[8][^{89}Zr]DFO-IgG or [^{89}Zr]DFO-YS5 with blocking YS5 group was observed at 3.3±1.0 %ID/gram ($p<0.01$) and 7.5±1.2 %ID/gram ($p<0.01$) respectively (Figure 4, Supplemental figure S4A). The data of tumor/non-target ratios in DU145 tumor targeting with [^{89}Zr]DFO-YS5 also showed the significant difference compared to [^{89}Zr]DFO-IgG control group (tumor/liver: $p<0.001$, tumor/kidney: $p=0.004$, tumor/spleen: $p<0.001$, tumor/muscle: $p<0.001$), and blocking group (tumor/liver: $p=0.021$, tumor/kidney: $p=0.002$, tumor/spleen: $p<0.001$, tumor/muscle: $p<0.001$).

In contrast to the high absolute tumor uptake observed in the DU145 model, much lower accumulation of [^{89}Zr]DFO-YS5 in MC38 (CD46-negative) tumors were observed at 96 h (Figure 4: C and D, Supplemental figure S4B, Supplemental table S4). Specifically, [^{89}Zr]DFO-YS5 uptake in the MC38 tumors at 96 h (MC38 vs. DU145: 4.7±2.3 vs. 14.8±6.4 %ID/gram, $p=0.026$) showed a statistically significant reduction in tracer accumulation, compared with uptake in CD46-positive DU145 tumors.

PET imaging and biodistribution of [^{89}Zr]DFO-YS5 and [^{68}Ga]PSMA-11 in DU145/22Rv1 dual tumor model

Next, we explored [^{89}Zr]DFO-YS5 and [^{68}Ga]PSMA-11 imaging in mice bearing DU145 and 22Rv1 xenografts, to determine the ability of the CD46 targeted agent to image PSMA negative prostate cancer. [^{89}Zr]DFO-IgG imaging was performed as a control agent to evaluate the enhanced permeability and retention (EPR) effect. As expected based on the single tumor experiments outlined above (Figures 3A and 3B), both DU145 and 22Rv1 showed high uptake of [^{89}Zr]DFO-YS5 (13.3 ± 3.9 %ID/gram and 11.2 ± 2.5 %ID/gram at 4 days post injection, Figures 5A and 5D, Supplemental table S5). The tumor/muscle ratio was 28.3 ± 9.3 and 23.1 ± 2.8, respectively. As a comparison, [^{89}Zr]DFO-IgG showed a moderate uptake in the DU145 and 22Rv1 xenografts, and the tumor/muscle ratio was much lower than the [^{89}Zr]DFO-YS5 group (Figures 5C, 5D and 5E, Supplemental table S5). In [^{68}Ga]PSMA-11 imaging (Figures 5F and 5G), the PSMA negative cell line DU145 showed low uptake (0.28 ± 0.06 % ID/gram) compared to the PSMA positive cell line 22Rv1 (4.04 ± 1.31 % ID/gram). An autoradiography study was performed after tumor was dissected demonstrated good uptake of [^{89}Zr]DFO-YS5 (Figure 5B, Supplemental figure S5). The distribution was not homogenous, probably because of the vasculature of the tumor, central necrosis, and/or the large size of the antibody. Taken together, these data demonstrate the feasibility of imaging CD46 positive, PMSA negative tumors with [^{89}Zr]DFO-YS5.

PET imaging and biodistribution of [^{89}Zr]DFO-YS5 in clinically relevant patient derived tumor models

We also tested the imaging ability of [^{89}Zr]DFO-YS5 in the LTL-331 patient derived adenocarcinoma xenograft model, and the LTL-331R and LTL545 neuroendocrine prostate cancer models[27]. In contrast with other xenograft models, these PDX tumors were grown in the more severely immunosuppressed NSG mouse model. Fc blocking was performed with excess cold IgG, reported to reduce Fc mediated splenic retention of antibody[29]. Despite Fc blocking, splenic retention of antibody was still greater than in the nu/nu model. Tumor

retention of the antibody was high in the LTL-331 model, measuring 18.8 ± 5.3 %ID/gram (Figures 6A and 6D, Supplemental table S6). Similar findings were seen in a bone metastasis model using the LTL-331 xenograft model, where tumor is introduced directly into the tibia by injection[30]. Similar to the subcutaneous xenograft model, a high degree of tumor uptake was observed (Supplemental figure S6). The neuroendocrine prostate model LTL-331R demonstrates a high degree of [^{89}Zr]DFO-YS5 uptake, slightly less than the LTL-331 model, measuring 12.5 ± 1.8 %ID/gram (Figure 6B, D, Supplemental table S6). The LTL-545 neuroendocrine prostate cancer demonstrated very high [^{89}Zr]DFO-YS5 uptake, measuring 32.0 ± 7.8% (Figure 6C, 6D, Supplemental table S6). We performed flow cytometry study to determine CD46 cell surface expression level, and found that all three PDXs express CD46, and LTL-545 expresses the highest level, with lower expression in LTL-331 and LTL-331R (Figure 6F), consistent with the result from PET imaging and biodistribution studies. These data demonstrated the utility of CD46 targeted imaging more clinically relevant patient derived xenograft models, suggesting feasibility for subsequent clinical translation. Moreover, they support the use of CD46 directed imaging and therapy in advanced, neuroendocrine prostate cancer phenotypes.

Discussion:

In this study we report a novel CD46-targeted immunoPET probe, [^{89}Zr]DFO-YS5, and its prostate cancer imaging abilities in multiple prostate cancer models, including mCRPC cell line xenografts (DU145 and 22Rv1), and PDX models with both adenocarcinoma (LTL-331) and neuroendocrine subtypes (LTL-331R, and LTL-545). The radiopharmaceutical could be synthesized in high yield, and *in vitro* study demonstrated that [^{89}Zr]DFO-YS5 has a high binding affinity for CD46. The *in vivo* study showed that this probe localized specifically at CD46 positive tumor with an excellent contrast to off-target organs. The specific binding of [^{89}Zr]DFO-YS5 to CD46 positive tumors was verified by appropriate control experiments including blocking, isotype control, and CD46 negative tumor imaging. The uptake of [^{89}Zr]DFO-YS5 in the CD46 negative MC38 xenograft and the uptake of a non-binding probe [^{89}Zr]DFO-IgG in the CD46 positive xenografts (DU145 and 22Rv1) were all low and close to 5% ID/gram. This moderate degree of uptake in these control groups compared to muscle or blood is attributed to the enhanced permeability and retention (EPR) effect of antibody in tumor[31]. To show key differentiating features of CD46 from lineage markers such as PSMA, we compared [^{89}Zr]DFO-YS5 with a PSMA-based imaging probe [^{68}Ga]PSMA-11. Importantly, [^{89}Zr]DFO-YS5 could detect PSMA negative/CD46 positive DU145 tumors. Finally, we demonstrated the ability to detect more clinically relevant human prostate cancer models including adenocarcinoma and neuroendocrine prostate cancer patient derived xenografts. In these models, we found that expression of CD46 measured with flow cytometry correlated with uptake of [^{89}Zr]DFO-YS5, with LTL545 being the highest, and lower expression in LTL-331 and LTL-331R. One important finding was that [^{89}Zr]DFO-YS5 had high uptake in neuroendocrine prostate cancer models LTL-331R and LTL-545, suggesting feasibility of detecting this aggressive prostate cancer phenotype. Taken together, these results demonstrate that [^{89}Zr]DFO-YS5 is an excellent imaging probe for detecting prostate cancer in preclinical models, spanning a wide variety of phenotypes, including adenocarcinoma, neuroendocrine prostate cancer, and PSMA negative tumors.

Our study differentiates from prior research performed with CD46 directed molecular imaging agents. One interesting feature of CD46 is that it is required for measles virus infection. Thus, viruses have been used to both image and treat CD46 positive prostate cancer using an oncolytic virus[32]. In the reporter gene strategy, a measles virus is genetically modified to induce overexpression of the sodium iodide symporter in the target cell[33]. The cancer cells could then be imaged with ^{123}I and treated with ^{131}I. While this strategy indicates feasibility of CD46 directed imaging and therapy in prostate cancer, clinical translation of this method would be challenging due to the requirement of the use of a virus in the imaging protocol. We previously labeled a single chain antibody fragment against CD46 with ^{99m}Tc, and imaged its biodistribution in mouse models using SPECT imaging[16]. The study showed high tumor uptake and tumor to blood (12:1) and tumor to muscle (70:1) ratios. However, when compared against the PET/CT method detailed herein, this prior study demonstrated inferior spatial resolution and imaging characteristics of SPECT imaging[16]. Moreover, a very high degree of renal uptake was observed. To overcome these challenges, we have labeled YS5, a novel internalizing full length antibody, with the positron emitting isotope ^{89}Zr. An additional advantage of this method is feasibility for subsequent clinical translation, given that an ADC using the YS5 platform is already in clinical trials. However, one important potential caveat is that the YS5 antibody does not cross react with murine CD46. Therefore, the mouse models presented herein may underestimate background uptake in human tissues. Additionally, PET imaging with full length antibodies also has important limitations. Notably, imaging is typically performed at least three days and up to one week after radiopharmaceutical injection, which may present a practical challenge for patients. Moreover, the use of long-lived isotopes such as ^{89}Zr also imparts greater radiation dose to patients. Nevertheless, ^{89}Zr antibody imaging is a promising overall method for tumor detection, with several agents now translated into the clinic[34–40].

Taken together, the data presented herein demonstrate that [^{89}Zr]DFO-YS5 is an effective radiopharmaceutical for imaging CD46 positive prostate cancer. CD46 is highly expressed in prostate cancer, including in metastatic prostate and treatment emergent small cell/neuroendocrine prostate cancer[17]. Theranostic targeting with PSMA is highly promising for both imaging and therapy for prostate cancer. However, PSMA expression is not uniform in prostate cancer, and some cases demonstrate either heterogeneous or absent PSMA expression[11–13]. Some PCa cells express low level of PSMA, which could not be detected through PSMA based imaging. Our imaging study in the dual DU145 and 22Rv1 model (Figure 5) mimics the situation sometimes seen in the clinic, with heterogeneous target expression[14]. Thus CD46 targeted imaging and therapy could be a more effective or complementary option for PSMA negative PCa.

Overall, the high reproducibility of labeling, high tumor expression, and high tumor uptake of [^{89}Zr]DFO-YS5 suggest a strong potential for translation of this imaging method to the clinic. A direct application of this probe could be a companion diagnostic to CD46-targeted therapy. With the CD46 ADC (FOR46, NCT03575819) now ongoing in multi-center phase I trials for mCRPC, a need may develop for appropriate selection of CD46 positive patients who will likely respond to therapy. CD46-targeted immunoPET imaging could be used to confirm CD46 expression in mCRPC in a quantitative manner, aid patient selection and

improve therapeutic outcomes in the ongoing or future trials. Similarly, these data also suggest feasibility for future CD46-directed radioligand therapy development.

Supplementary Material

Refer to Web version on PubMed Central for supplementary material.

Acknowledgments:

This work was supported by grants from the NIH/National Cancer Institute R01CA223767 (BL and JH), CCSG P30 CA44579 (University of Virginia Cancer Center). Part of the PET imaging data was acquired through the University of Virginia Molecular Imaging Core Lab, with NIH S10OD021672 funding for the Albira Si trimodal scanner. RRF was supported by a David Blitzer Prostate Cancer Foundation Young Investigator Award, a UCSF Research Allocation Program Precision Imaging of Cancer and Therapy Award (funded by UCSF Cancer Center Support Grant P30CA082103), and the Prostate Cancer Research Program of the Congressionally Directed Medical Research Programs (DOD CDMRP) PC190656. MALDI MS data was provided by the Mass Spectrometry Facility, Department of Chemistry, University of Alberta, Edmonton, AB, Canada.

References

1. Fanti S, Minozzi S, Antoch G, et al. Consensus on molecular imaging and theranostics in prostate cancer. Lancet Oncol. 2018;19:e696–e708. [PubMed: 30507436]
2. Current K, Meyer C, Magyar CE, et al. Investigating PSMA-Targeted Radioligand Therapy Ef fi cacy as a Function of Cellular PSMA Levels and Intratumoral PSMA Heterogeneity. Clin Cancer Res. doi:10.1158/1078-0432.CCR-19-1485.
3. Hammer S, Hagemann UB, Zitzmann-kolbe S, et al. Preclinical efficacy of a PSMA-targeted thorium-227 conjugate (PSMA-TTC), a targeted alpha therapy for prostate cancer. Clin Cancer Res. 2020;26:1985–96. [PubMed: 31831560]
4. Sharma SK, Glaser JM, Edwards KJ, et al. A systematic evaluation of antibody modification and radiolabeling for optimized immuno-PET. Bioconjugate Chem. doi:10.1021/acs.bioconjchem.0c00087
5. Holland JP, Divilov V, Bander NH, Smith-jones PM, Larson SM, Lewis JS. ^{89}Zr-DFO-J591 for immunoPET of prostate-specific membrane antigen expression *in vivo*. J Nucl Med 2010; 51:1293–1300. [PubMed: 20660376]
6. Eder M, Schäfer M, Bauder-Wüst U, et al. ^{68}Ga-complex lipophilicity and the targeting property of a urea-based PSMA inhibitor for PET imaging. Bioconjugate Chem. 2012;23:688–97.
7. Fendler WP, Rahbar K, Herrmann K, Kratochwil C, Eiber M. ^{177}Lu-PSMA radioligand therapy for prostate cancer. J Nucl Med 2017;58:1196–1200. [PubMed: 28663195]
8. Kratochwil C, Bruchertseifer F, Giesel FL, et al. ^{225}Ac-PSMA-617 for PSMA-targeted α-radiation therapy of metastatic castration-resistant prostate cancer. J Nucl Med 2016; 57:1941–44. [PubMed: 27390158]
9. Dannoon S, Ganguly T, Cahaya H, et al. Structure-activity relationship of ^{18}F-labeled phosphoramidate peptidomimetic prostate-specific membrane antigen (PSMA)-targeted inhibitor analogues for PET imaging of prostate cancer. J Med Chem. 2016;59:5684–94. [PubMed: 27228467]
10. Hrkach J, Von Hoff D, Ali MM, et al. Preclinical development and clinical translation of a PSMA-targeted docetaxel nanoparticle with a differentiated pharmacological profile. Sci Transl Med 2012;4:128–39.
11. Mannweiler S, Amersdorfer P. Heterogeneity of prostate-specific membrane antigen (PSMA) expression in prostate carcinoma with distant metastasis. Pathol Oncol Res 2009;15:167–72. [PubMed: 18802790]
12. Alberts I, Sachpekidis C, et al. PSMA-negative prostate cancer and the continued value of choline-PET/CT 2020;59:33–4.

13. Ferdinandus J, Violet J, Sandhu S, et al. Prognostic biomarkers in men with metastatic castration-resistant prostate cancer receiving ^{177}Lu-PSMA-617. Eur J Nucl Med Mol Imaging 2020;6–11. [PubMed: 33037451]
14. Paschalis A, Sheehan B, Riisnaes R, et al. Prostate-specific membrane antigen heterogeneity and DNA repair defects in prostate cancer. Eur Urol 2019;76:469–78. [PubMed: 31345636]
15. Ruan W, Sassoon A, An F, Simko JP, Liu B. Identification of clinically significant tumor antigens by selecting phage antibody library on tumor cells in situ using laser capture microdissection. Mol Cell Proteomics 2006;5:2364–73. [PubMed: 16982673]
16. He J, Wang Y, Feng J, et al. Targeting prostate cancer cells in vivo using a rapidly internalizing novel human single-chain antibody fragment. J Nucl Med 2010;51:427–32. [PubMed: 20150269]
17. Su Y, Liu Y, Behrens CR, et al. Targeting CD46 for both adenocarcinoma and neuroendocrine prostate cancer. JCI Insight 2018;3.
18. Geller A, Yan J. The role of membrane bound complement regulatory proteins in tumor development and cancer immunotherapy. Front Immunol 2019;10:1–13. [PubMed: 30723466]
19. Guillerme JB, Boisgerault N, Roulois D, et al. Measles virus vaccine-infected tumor cells induce tumor antigen cross-presentation by human plasmacytoid dendritic cells. Clin Cancer Res 2013;19:1147–58. [PubMed: 23339127]
20. Sherbenou DW, Aftab BT, Su Y, et al. Antibody-drug conjugate targeting CD46 eliminates multiple myeloma cells. J Clin Invest 2016;126:4640–53. [PubMed: 27841764]
21. Knowles SM, Wu AM. Advances in immuno-positron emission tomography: antibodies for molecular imaging in oncology. J Clin Oncol 2012;30:3884–92. [PubMed: 22987087]
22. Wei W, Rosenkrans ZT, Liu J, Huang G, Luo QY, Cai W. ImmunoPET: concept, design, and applications. Chem Rev 2020;120:3787–851. [PubMed: 32202104]
23. Verel I, Visser GWM, Boellaard R, Walsum MS Van, Snow GB, Van Dongen GAMS. ^{89}Zr immuno-PET: comprehensive procedures for the production of ^{89}Zr-labeled monoclonal antibodies. J Nucl Med 2003;44:1271–81. [PubMed: 12902418]
24. Deri MA, Zeglis BM, Francesconi LC, Lewis JS. PET imaging with ^{89}Zr: From radiochemistry to the clinic. Nucl Med Biol 2013;40:3–14. [PubMed: 22998840]
25. Bensch F, van der Veen EL, Lub-de Hooge MN, et al. ^{89}Zr-atezolizumab imaging as a non-invasive approach to assess clinical response to PD-L1 blockade in cancer. Nat Med 2018;24:1852–8. [PubMed: 30478423]
26. Beckford-vera DR, Gonzalez-junca A, Janneck JS, et al. PET/CT imaging of human TNF α using [^{89}Zr] Certolizumab pegol in a transgenic preclinical model of rheumatoid arthritis. Mol Imaging Biol 2020;22:105–14. [PubMed: 31065895]
27. Lin D, Wyatt AW, Xue H, et al. High fidelity patient-derived xenografts for accelerating prostate cancer discovery and drug development. Cancer Res 2014;74:1272–83. [PubMed: 24356420]
28. Wang S, Blaha C, Santos R, et al. Synthesis and initial biological evaluation of boron-containing prostate-specific membrane antigen ligands for treatment of prostate cancer using boron neutron capture therapy. Mol Pharmaceutics 2019;16:3831–41.
29. Sharma SK, Chow A, Monette S, et al. Fc-mediated anomalous biodistribution of therapeutic antibodies in immunodeficient mouse models. Cancer Res 2018;78:1820–32. [PubMed: 29363548]
30. Corey E, Quinn JE, Bladou F, et al. Establishment and characterization of osseous prostate cancer models: Intra-tibial injection of human prostate cancer cells. Prostate 2002;52:20–33. [PubMed: 11992617]
31. Thurber MG. Weissleder R. Quantitating antibody uptake *in vivo*: Conditional dependence on antigen expression levels. Mol Imaging Biol. 2011;13:623–32. [PubMed: 20809210]
32. Msaouel P, Iankov ID, Allen C, et al. Engineered measles virus as a novel oncolytic therapy against prostate cancer. 2009;69:82–91.
33. Msaouel P, Iankov ID, Allen C, et al. Noninvasive imaging and radiovirotherapy of prostate cancer using an oncolytic measles virus expressing the sodium iodide symporter. Mol Ther 2009;17:2041–48. [PubMed: 19773744]
34. Doran MG, Watson PA, Cheal SM, et al. Annotating STEAP1 regulation in prostate cancer with ^{89}Zr immuno-PET. J Nucl Med 2014;55:2045–49. [PubMed: 25453051]

35. Carrasquillo JA, Fine BM, Pandit-Taskar N, et al. Imaging patients with metastatic castration-resistant prostate cancer using ^{89}Zr-DFO-MSTP2109A anti-STEAP1 antibody. J Nucl Med 2019;60:1517–23. [PubMed: 31053681]

36. Knowles SM, Zettlitz KA, Tavaré R, et al. Quantitative immunoPET of prostate cancer xenografts with ^{89}Zr- and ^{124}I-labeled Anti-PSCA A11 minibody. J Nucl Med 2014;55:452–9. [PubMed: 24504052]

37. Morris MJ, Eisenberger MA, Pili R, et al. A phase I/IIA study of AGS-PSCA for castration-resistant prostate cancer. Ann Oncol 2012;23:2714–9. [PubMed: 22553195]

38. Li M, Jiang D, Barnhart TE, et al. Immuno-PET imaging of VEGFR-2 expression in prostate cancer with ^{89}Zr-labeled ramucirumab. Am J Cancer Res 2019;9:2037–46. [PubMed: 31598404]

39. Hintz HM, Gallant JP, Vander Griend DJ, Coleman IM, Nelson PS, LeBeau AM. Imaging fibroblast activation protein alpha improves diagnosis of metastatic prostate cancer with positron emission tomography. Clin Cancer Res 2020; doi:10.1158/1078-0432.ccr-20-1358.

40. Glumac PM, Gallant JP, Shapovalova M, et al. Exploitation of CD133 for the targeted imaging of lethal prostate cancer. Clin Cancer Res 2020;26:1054–64. [PubMed: 31732520]

Translational Relevance

Despite recent progress, metastatic castration-resistant prostate cancer (mCRPC) remains incurable. We recently identified CD46 as a novel lineage independent mCRPC cell surface antigen with high expression in aggressive, late stage and treatment-resistant PCa. Herein, we developed [^{89}Zr]DFO-YS5 as a CD46 immunoPET imaging probe, and demonstrated that [^{89}Zr]DFO-YS5 imaged both CD46 positive tumor cell line xenografts and patient-derived xenografts with excellent contrast. With a CD46-targeted antibody-drug conjugate (FOR46) currently in phase I trials, this CD46-targeting immunoPET radiotracer could be translated to clinical studies rapidly, aiding patient selection and/or assessment of treatment response.

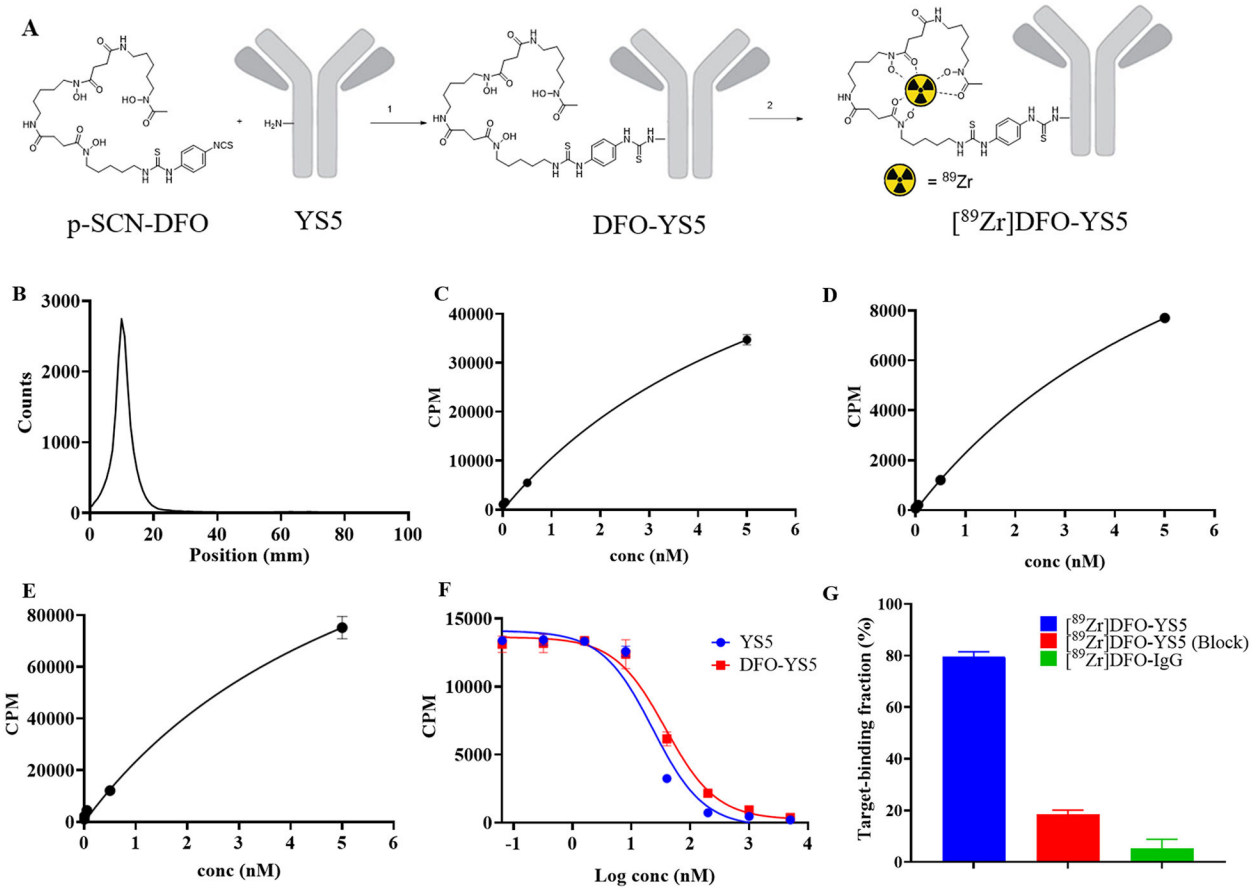

Figure 1:

Synthesis and *in vitro* analysis of [^{89}Zr]DFO-YS5. A) Synthesis scheme of [^{89}Zr]DFO-YS5. Reaction conditions: 1) 0.1M Na_2CO_3-$NaHCO_3$ buffer pH 9.0, 37 °C, 45 min. 2) 2M NH_4OAc, rt, 1 h. B) iTLC analysis of [^{89}Zr]DFO-YS5, demonstrating greater than 98% purity. C) K_d measurement of [^{89}Zr]DFO-YS5 on DU145 cell line determined by a saturation binding assay (K_d = 6.7 ± 0.3 nM). D) K_d measurement of [^{89}Zr]DFO-YS5 on 22Rv1 cell line determined by a saturation binding assay (K_d = 7.2 ± 0.9 nM). E) K_d measurement of [^{89}Zr]DFO-YS5 on CD46 recombinant protein determined by a saturation binding assay (K_d = 6.0 ± 0.6 nM). F) Competition radioligand binding assay using [^{89}Zr]DFO-YS5, demonstrating similar IC50 for YS5 vs. DFO-YS5 (23.1 ± 1.8 and 37.8 ± 2.5 nM, respectively). G) Magnetic bead based radioligand binding assay, demonstrating target binding fraction of 79.5 ± 2.0% for [^{89}Zr]DFO-YS5.

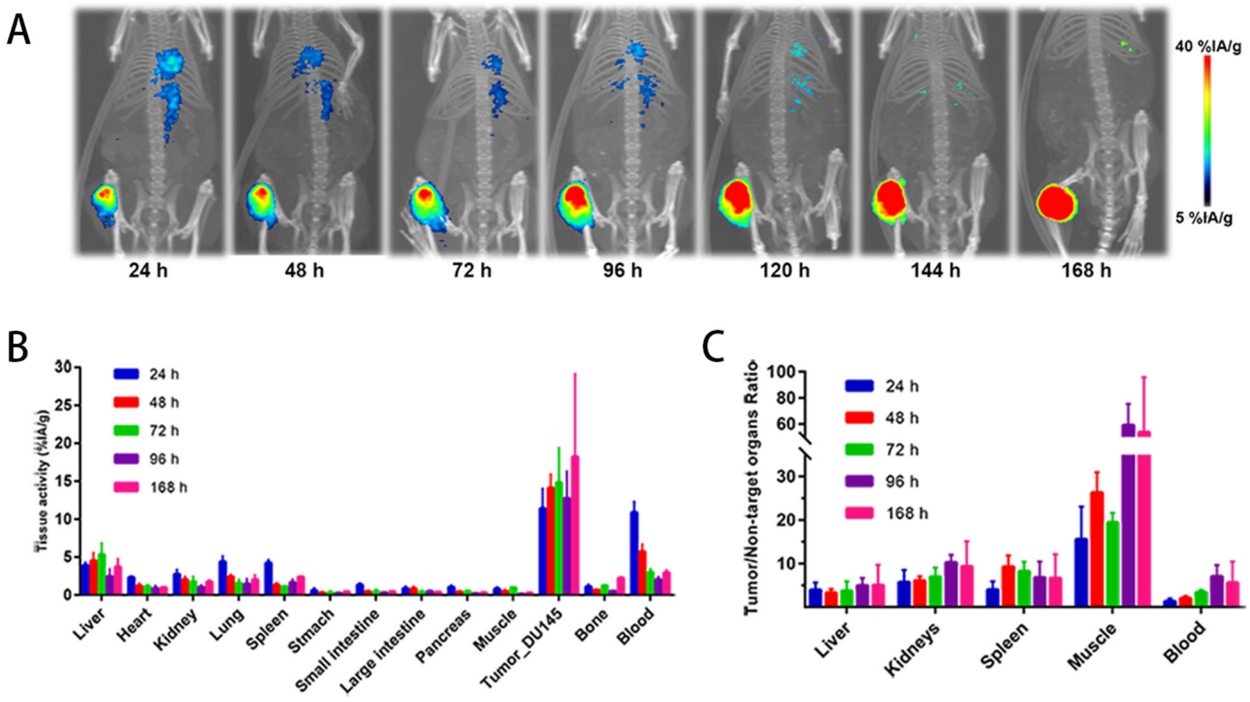

Figure 2.

[^{89}Zr]DFO-YS5 detects tumors in male nu/nu mice with subcutaneous DU145 xenografts. A) Maximum intensity projections of [^{89}Zr]DFO-YS5 from 24 h to 168 h. B) Biodistribution of [^{89}Zr]DFO-YS5 in various tissues at time points from 24 h to 168 h. C) Tumor/Non-target organ ratio of [^{89}Zr]DFO-YS5 from 24 h to 168 h.

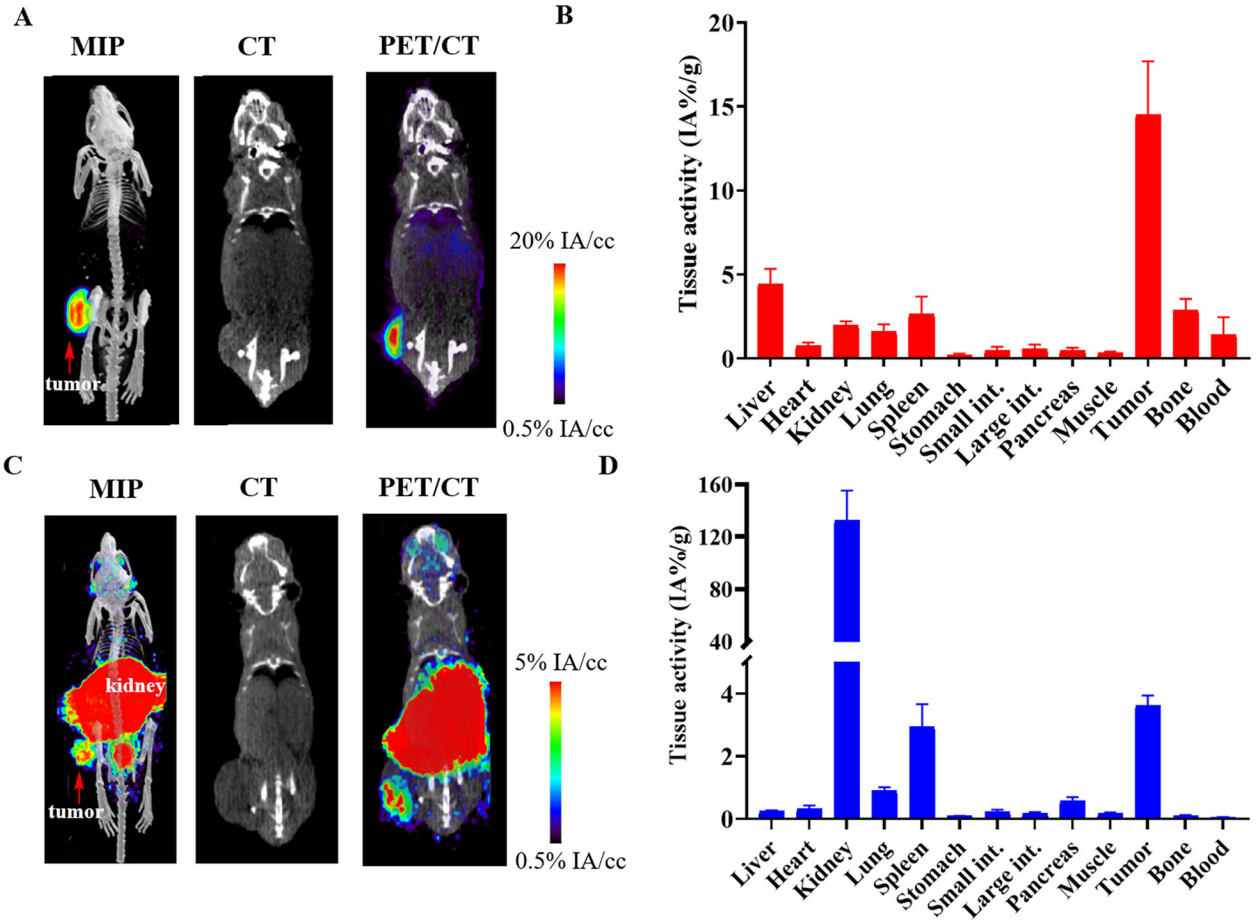

Figure 3:

[^{89}Zr]DFO-YS5 and [^{68}Ga]PSMA-11 imaging and biodistribution in the 22rV1 xenograft model reveals favorable imaging characteristics for [^{89}Zr]DFO-YS5. A) Maximum intensity projection PET/CT, coronal CT, and μPET/CT fusion images obtained 7 days following administration of [^{89}Zr]DFO-YS5 reveal high tumor uptake with low background tissue retention. B) Biodistribution analysis of [^{89}Zr]DFO-YS5 in 22Rv1 xenografts obtained 7 days following administration of [^{89}Zr]DFO-YS5, demonstrate high tumor retention. C) Maximum intensity projection PET/CT, coronal CT, and μPET/CT fusion images obtained 60 minutes following administration of [^{68}Ga]PSMA-11 reveal high tumor uptake with expected high abdominal radiotracer accumulation. D) Biodistribution analysis of obtained 60 minutes following administration of [^{68}Ga]PSMA-11 reveals high tumor, spleen, and kidney uptake.

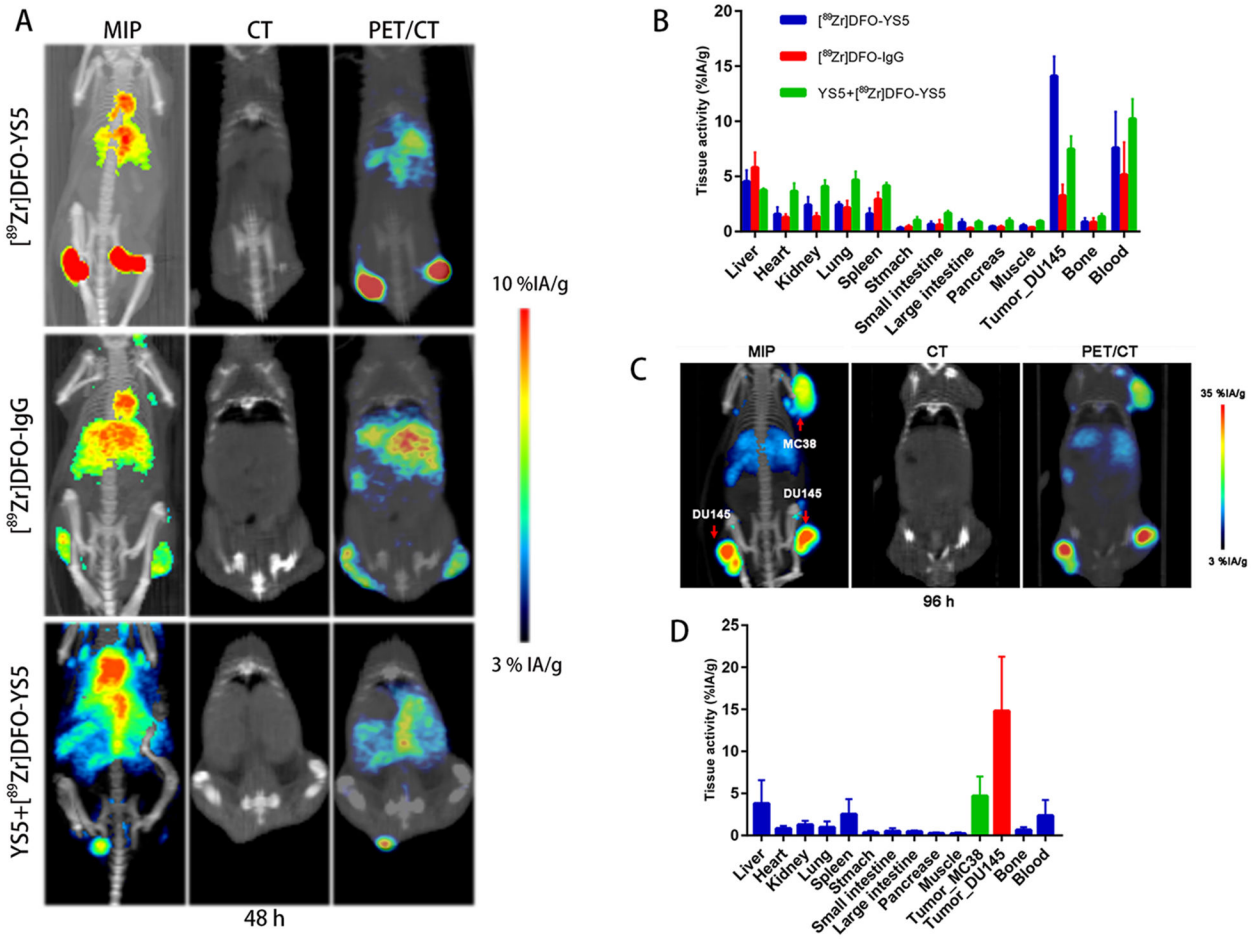

Figure 4:

[89Zr]DFO-YS5 targeting specificity in subcutaneous tumor models. A) Maximum intensity projections and μPET/CT of [89Zr]DFO-YS5, [89Zr]DFO-IgG and blocking YS5+[89Zr]DFO-YS5 in DU145 subcutaneous xenograft tumor mice at 48 h. B) Biodistribution of [89Zr]DFO-YS5, [89Zr]DFO-IgG and YS5+[89Zr]DFO-YS5 in DU145 subcutaneous xenograft tumor mice at 48 h. C) Maximum intensity projections and μPET/CT of [89Zr]DFO-YS5 in male nu/nu mice with subcutaneous DU145 and MC38 xenograft at 96 h. D) Biodistribution of [89Zr]DFO-YS5 in male nu/nu mice with subcutaneous DU145 and MC38 xenograft at 96 h.

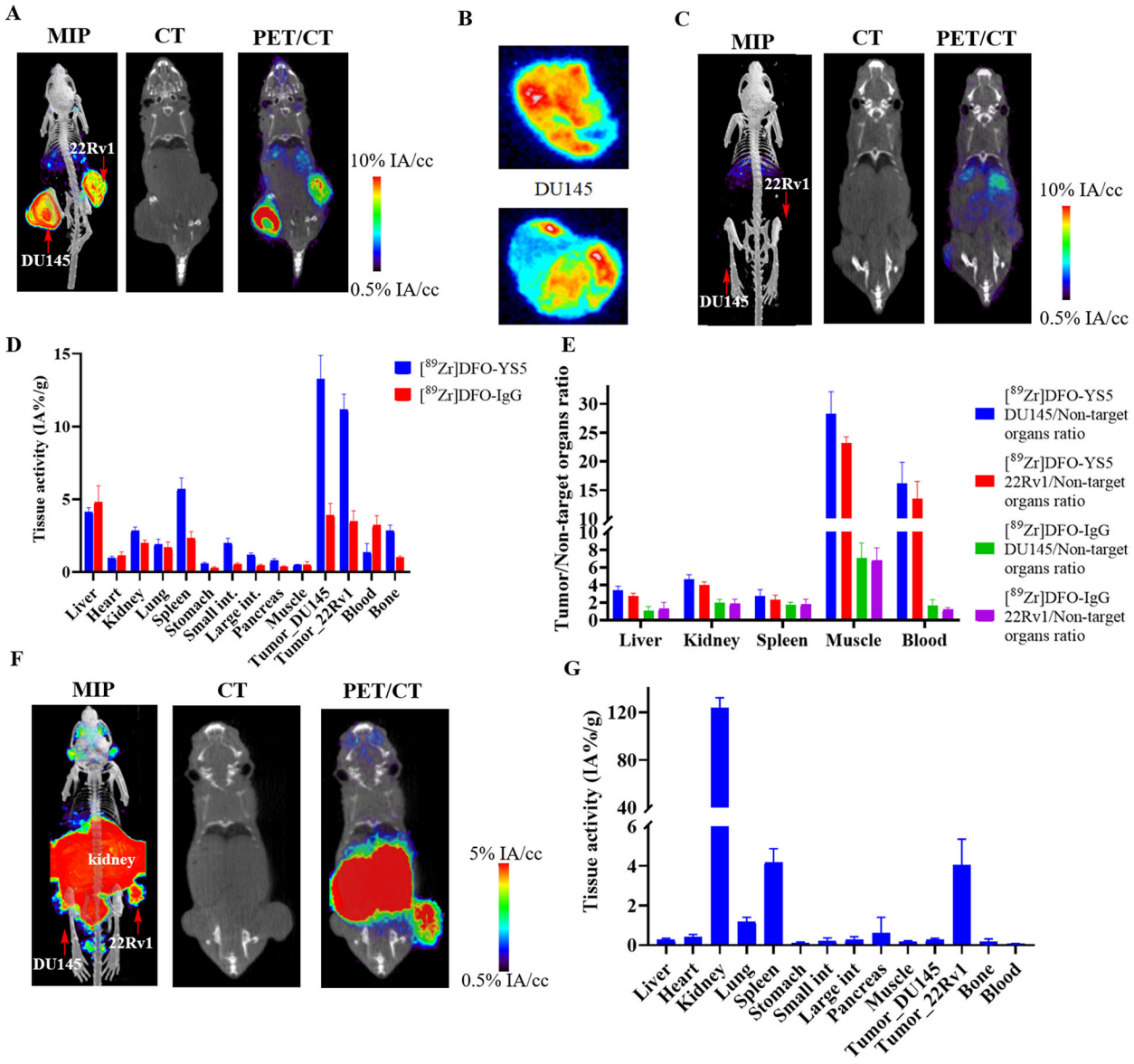

Figure 5:

Comparison of [^{89}Zr]DFO-YS5 and [^{68}Ga]PSMA-11 PET in a dual 22Rv1 and DU145 PCa tumor model demonstrates feasibility for imaging PSMA negative tumors with PET/CT. A) Maximum intensity projection PET/CT, coronal CT and coronal μPET/CT slices obtained 4 days after administration of [^{89}Zr]DFO-YS5 reveal high tumor uptake. B) Autoradiography of 22Rv1 and DU145 tumor sections. C) Maximum intensity projection PET/CT, coronal CT and coronal μPET/CT slices obtained 4 days after administration of [^{89}Zr]DFO-IgG reveal low tumor uptake. D) Biodistribution of [^{89}Zr]DFO-YS5 and [^{89}Zr]DFO-IgG. E) Tissue/Organ ratio of [^{89}Zr]DFO-YS5 and [^{89}Zr]DFO-IgG biodistribution. F) Maximum intensity projection PET/CT, coronal CT and coronal μPET/CT slices obtained 60 minutes after administration of [^{68}Ga]PSMA-11 reveal high tumoral uptake in 22Rv1, but low in DU145. G) Biodistribution data matching imaging data in panel F.

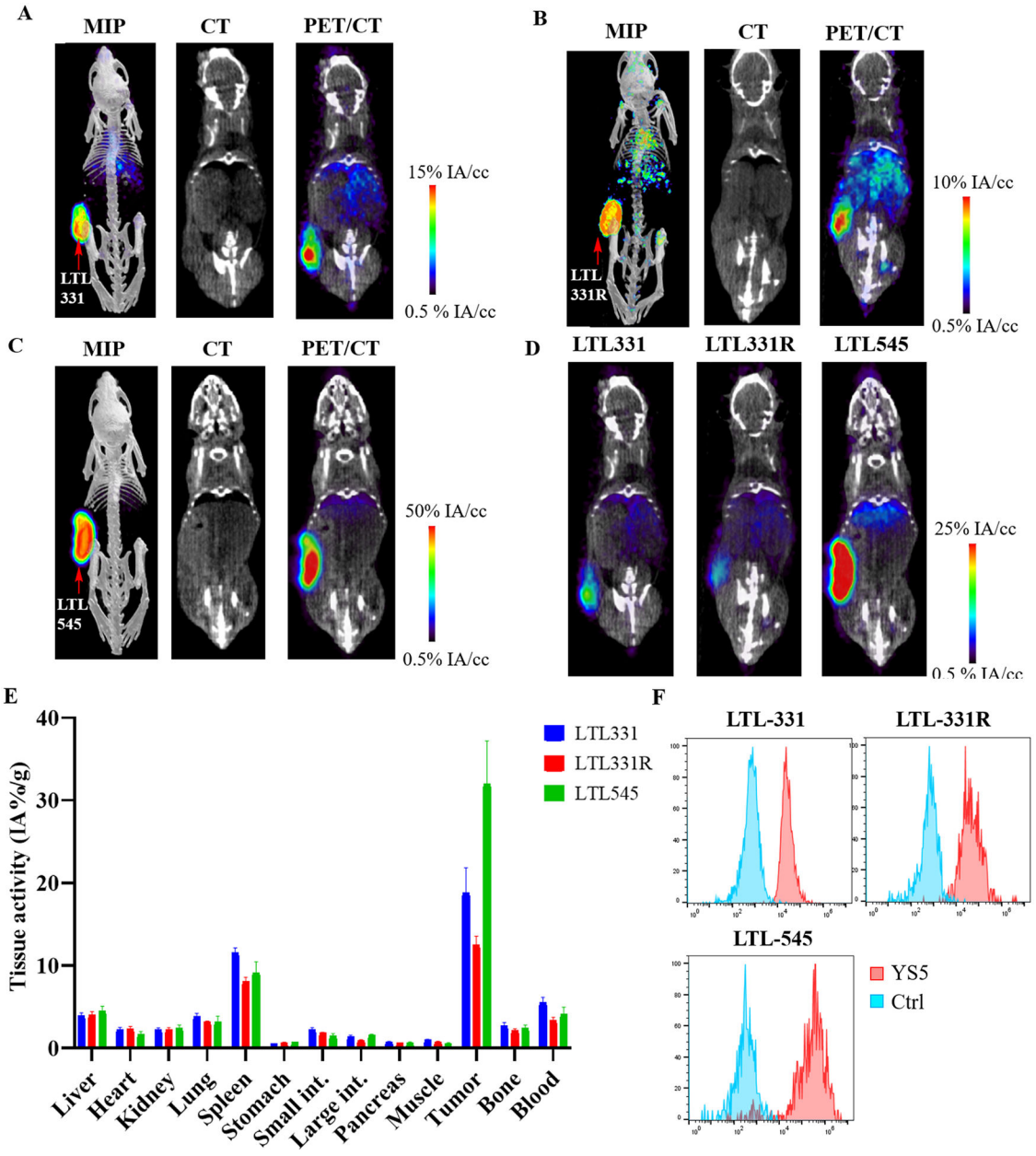

Figure 6:

PET imaging of [^{89}Zr]DFO-YS5 detects tumors in a patient derived xenograft models, including in neuroendocrine prostate cancer. Maximum intensity projection PET/CT, coronal CT and coronal μPET/CT slices obtained 4 days after administration of [^{89}Zr]DFO-YS5 in the A) LTL-331, B) LTL-331R, and C) LTL-545 tumor models. D) Micro PET/CT fusion images on the same scale, demonstrating greater uptake in the LTL-545 model when compared against LTL-331 or 331-R. E) Biodistribution analysis obtained 4 days after administration of [^{89}Zr]DFO-YS5 reveal high tumor uptake in the xenograft models, particularly for the LTL-545 neuroendocrine prostate cancer. F) Flow cytometry analysis of CD46 cell surface expression in PDXs. MFI values for LTL-331 (adenocarcinoma),

LTL-331R (neuroendocrine), and LTL-545 (neuroendocrine) are 40,804, 40,473, and 286,645, respectively. Ctrl: an isotype matched non-binding antibody control.